Food Chemistry xxx (xxxx) xxxx

Contents lists available at ScienceDirect

Food Chemistry

journal homepage: www.elsevier.com/locate/foodchem

Ultra-sensitive electrochemical aptasensor for label-free detection of Aflatoxin B1 in wheat flour sample using factorial design experiments

Faezeh Rahimi, Hamideh Roshanfekr*, Hossein Peyman

Department of Chemistry, Ilam Branch, Islamic Azad University, Ilam, Iran

ARTICLE INFO

Keywords:
Biosensor
Mycotoxin
Carbon quantum dots
Octahedral Cu_2O
Taguchi method

ABSTRACT

Considering the significance of mycotoxin detection in food industries, herein, an ultrasensitive aptasensor was developed based on aflatoxin B1 aptamer immobilized on Carbon quantum dots/octahedral Cu_2O nanocomposite. Electrochemical measurements were based on Electrochemical Impedance Spectroscopy (EIS) and Differential Pulse Voltammetry (DPV). Since the effective parameters (pH, temperature, incubation time and concentration of aptamers) are interdependent, so their dependent study can be nonideal. Taguchi method has solved this problem and optimized the experimental conditions using a smaller number of experiments. Under optimum conditions, the electrochemical signals declined as AFB1 concentrations increased with a dynamic range of 3 $ag.ml^{-1}$ -1.9 $\mu g.ml^{-1}$ and a low limit of detection (LOD) of 0.9 $\pm$ 0.04 ag ml^{-1}. The obtained results proved sufficient repeatability (RSD = 2.4%), reproducibility (RSD = 2.56%), accuracy (97.2–104.4% recovery), and robustness (RSD = 3.25%). Furthermore, considerable selectivity, stability and reliability of the aptasensor confirmed the capability to work in future real assays.

1. Introduction

Aflatoxins (AFs) are poisonous substances that can contaminate food crops. They have produced by two closely related species of fungi: *Aspergillus flavus* and *A. parasiticus*. There are several types of AF (14 or more) in nature, but four AFs B1, B2, G1, and G2 are particularly dangerous to humans and animals as they have been found in all major food crops; but most human exposure comes from contaminated nuts, grains, and their derived products. Moreover, the AFs of M1 and M2 are metabolites resulted from the hydroxylation of B1 and B2 AFs, respectively, which can be found in milk in areas of high AF exposure. Among the mycotoxins, AFB1 is the most common toxic compound in food and it also has the highest toxicity due to its high ability to attach to DNA and proteins (Mirian, Khanahmad, Darzi, Salehi, & Sadeghi-Aliabadi, 2017). In human carcinogens, by the International Agency for Research on Cancer (IARC), AFB1 has been arranged in categories of Group 1(Hernandez-Vargas et al., 2015). Therefore, developing and creating a quick and sensitive procedure for the diagnosis of AFB1 is essential for the health and safety of the food chain.

Up to now, several diagnostic methods have been employed to AFB1 detection such as liquid chromatography-mass spectrometry (LC-MS), high-performance liquid chromatography (HPLC) and spectrofluorimetric (Hashemi & Taherimaslak, 2014; Hashemi, Taherimaslak, & Rashidi, 2014; Liu, Jin, Sun, Ma, & Lin, 2012). Nonetheless, some of these methods suffer from several restrictions such as the utilization of substantial volumes of samples, complicated sample pretreatment stages, and low sensitivity. Accordingly, a superseded way with lower utilizing cost and adequate detection rapidity to the evaluation of the low amounts of AFB1 is an electrochemical technique. Several electrochemical evaluations have been applied to date involve connecting sensors and biosensors(Farmani, Peyman, & Roshanfekr, 2020; Heydarzadeh, Roshanfekr, Peyman, & Kashanian, 2020; Peyman, Roshanfekr, & Ansari, 2020) (Abnous et al., 2017; Azri, Selamat, & Sukor, 2017; Geleta, Zhao, & Wang, 2018; Wang et al., 2012; Wu, Wei, Wei, Liu, & Liu, 2019; Yagati, Chavan, Baek, Lee, & Min, 2018; Zhang et al., 2016).

Among the various types of biosensors, the use of aptamers as a biosensing element has attracted much attention in recent years. The aptamers are short nucleic acids (DNA or RNA) sequences, including the 15–90 single-stranded of oligonucleotides, with improved affinity to various targets as proteins, cells, and viruses (Mirian et al., 2017). In this area, they have shown good results as well as in other sciences such as pharmacy, advanced systems drug delivery, and identification of new drugs and assessment of their biological activity (Ilgu & Nilsen-Hamilton, 2016; Mishra, Sharma, & Mishra, 2018).

Metal nanoparticles used to manufacture of sensors have shown

* Corresponding author.
E-mail address: roshanfekrhamide@gmail.com (H. Roshanfekr).

https://doi.org/10.1016/j.foodchem.2020.128436
Received 3 May 2020; Received in revised form 14 October 2020; Accepted 16 October 2020
0308-8146/ © 2020 Elsevier Ltd. All rights reserved.

Please cite this article as: Faezeh Rahimi, Hamideh Roshanfekr and Hossein Peyman, Food Chemistry, https://doi.org/10.1016/j.foodchem.2020.128436

high electrocatalytic activity in the detection of analytes (Sharma et al., 2016). Cuprous oxide (Cu_2O) nanoparticles as a p-type semiconductor have many usages in different areas, like electrochemical sensors, photochemical catalysis, and biosensors. Furthermore, the carbon quantum dots (CQDs) recently, as a unique and new nano-carbons class, have gained significant consideration due to the abundant chemical or physical attributes, like the nonpoisonous, photoinduced electron transfer, water-solubility, luminescence, redox attributes, and great stability. In the present study, CQDs-Cu_2O nanocomposite is used to increase the immobilization efficiency of aptamers. Findings on different studies have been shown that the increased immobilization efficiency causes more electron transfer and increase the aptasensor sensitivity (He, Li, Liu, Huang, Kang, & Lee, 2011).

Taguchi method (TM) is a statistical approach to optimize the process parameters, that is developed by Taguchi and Konishi. A precise choice of method factors and dividing them into control factors and noise factors is the key step to reach the favorable results. The obtained results of the TM calculations are applied to investigate the data and forecast the quality of the designed method (Athreya & Venkatesh, 2012). The design of an experiment involves selecting the most appropriate conditions, determining the factors with the appropriate levels, and finally explaining the combinations of experiments (Phadke, 1995).

Herein, combining with the good electrochemical performance of octahderal Cu_2O and the water solubility and biocompatibility of CQDs, we prepared a proper platform to an effective immobilization of AFB1 aptamers using interaction between amine groups of aptamers and carboxylic groups of nanocomposites. The present work, for the first time, investigates the influence of the effective experimental parameters on multi-performance characteristics in constructed electrochemical aptasensor using TM for AFB1 detection.

2. Experimental section

2.1. Apparatus

All of the electrochemical evaluations were performed with a μAutolab (PGSTAT302N, Utrecht, The Netherlands) potentiostat–galvanostat equipped with NOVA (1.11) software at room temperature. This system is coupled to the FRA32 to recorde the impedance analysis module. The electrochemical studies were carried out by Aptamer/Cu_2O-CQDs/GCE as a working electrode. Ag/AgCl electrode (saturated KCl) as a reference electrode and a platinum wire as the auxiliary electrode. The pH tests were accomplished using pH-meter (Metrohm Model 691) with a glass electrode during the evaluations. In these experiments to dispersion of the particles in the solution for -obtain uniform nano-sized materials an ultrasonic bath (euronda, eurosonic® 4D) was employed. The synthesized NPs for modification of electrode were characterized by FTIR spectroscopy (model ALPHA, Bruker, Germany), EDS (MIRA3 LM model, Brno, Czech Republic) with applying an accelerating voltage 15 kV, FE-SEM (model MIRA III, TESCAN Co., Czech) and XRD (PHILIPS model PW1730).

2.2. Reagents

Glucose, sodium dodecyl sulfate (SDS), hydrochloric acid (HCl), sodium hydroxide (NaOH), copper (II) chloride dehydrate ($CuCl_2{\cdot}2H_2O$), hydroxylamine hydrochloride ($NH_2OH{\cdot}HCl$) and the Certified Reference Materials (CRMs) were purchased from Merck Co. (Darmstadt, Germany). The AFB1 was acquired from Sigma -Aldrich. For the preparation of aqueous solutions, we used deionized water. In these experiments, H_3PO_4, KH_2PO_4, and K_2HPO_4 salts were applied to the preparation of phosphate buffer solutions (PBS) (0.1 M). The NaOH and HCl solutions were used to adjust the pH. The whole of tests was performed at room temperature. The synthetic AFB1 aptamer with the sequence of [5′-TGG GGT TTT GGT GGC GGG TGG TGT ACG GGC GAA GG-(NH_2)-3′ with an amine group at the 3′ end, was obtained from Takapoozist (Iran). The standard solution of aptamer (100 μM) was prepared in PBS (pH = 7.4) and then frozen for fresh utilization. The standard solution of AFB1 in acetonitrile (10 μM) was prepared, and then the prepared standard solutions stored at 4 °C for further utilization.

2.3. Preparation of the CQDs

The CQDs were synthesized by hydrothermal oxidation of carbohydrates (glucose) with acid/alkali additives: initially, 1.0 gr glucose and 0.1 gr NaOH were dissolved in 15 ml distilled water under stirring. Then the solution was heated at 160 °C for 4 h in a Teflon-lined stainless-steel autoclave. After cooling the resulting solution, centrifugation of the acquired solution was accomplished at 10000 rpm for 2 min and the desired product was obtained. The process was followed by heating at 100 °C to dissolve out of the remaining sodium hydroxide (purification step). After that, the filtration of the solution was performed through a 0.45 μm Milli-pore filter, and the final product dried under vacuum. The resulting CQDs in the form of a clear solution was kept into the deionized water. Here, glucose and NaOH were used as the source of carbon substance and an additive, respectively. The UV–Vis and fluorescence spectra of CQDs were taken and their maximum wavelengths (λ_{max}) at 280 and 450 nm, respectively, were confirmed the synthesized CQDs NPs with two techniques (data are not shown).

2.4. Production of the Cu_2O and Cu_2O/CQDs nanocomposites

To prepare the octahedral Cu_2O, at first, NaOH (8 ml, 1 M) and $CuCl_2$ (4 ml, 0.1 M) solutions were appended into 364 ml deionized water while the solution was stirring strongly. Afterward, a light blue fluffy precipitate was created instantly. Then, SDS powder (3.532 g) was added to the above solution until the dissolution of the powder under vigorous stirring. Next, the acquired solution was mixed with 24 ml $NH_2OH{\cdot}HCl$ (0.2 M), while the solution was stirring, and a yellow solution was formed. The obtained solution was exposed to the air for 2 h and after 50 min sonication, the final solution was centrifuged at 10000 rpm for 5 min until the solution becomes clear. The centrifugation of obtained precipitates (octahedral Cu_2O) again was performed by ethanol twice more and, finally dispersion of precipitates was carried out in ethanol for the next evaluations.

To synthesis octahedral Cu_2O/CQDs nanocomposites, the final solution above (a yellow solution) before sonication slowly added into a mixture of 25 ml glucose (1.0 M) and 25 ml NaOH (1.0 M). Afterward, ultrasonication of this solution was accomplished for 10 min; then the acquired solution was exposed to air for 1 h, after maintaining in ultrasonic for 50 min. The centrifugation of the final solution was carried out at 5000 rpm for 5 min until the solution becomes clear. The centrifugation of precipitates (octahedral Cu_2O-CQDs nanocomposites) were accomplished twice more in ethanol again and eventually for the next experiments were dispersed in ethanol (Li, Zhong, Zhang, Weng, & Li, 2015).

2.5. Preparing of the aptasensor

The GCE was firstly polished using 0.3 and 0.05 μm alumina slurry to a mirror-like and next was rinsed by alcohol and deionized water consecutively in an ultrasonic bath. For the making of the mentioned aptasensor, at first 1 mg of octahedral Cu_2O-CQDs nanocomposites dispersed in 1 ml ethanol, and the solution was placed in an ultrasonic bath for 30 min to ensure the uniformity of octahedral Cu_2O-CQDs nanocomposites. Then 10 μl of the obtained suspension was dropped onto the surface of GCE and dried at room temperature to form a Cu_2O-CQDs/GCE. Then, deionized water was used to washing the fabricated sensor and next, this electrode dipped into the 1 ml buffer solution containing 10 μM aptamer for 24 h. Aptamers as probe molecules

immobilized on the Cu_2O-CQDs/GCE surface due to the chemisorption process between amine groups of aptamers and functional groups (carboxyl and hydroxyl groups) on the electrode surface. The plentiful presence of functional groups, especially carboxyl groups in the CQDs provided strong bonding of aptamers on the surface of CQDs with π-π interactions (Miao, Wang, Zhuo, Zhou, & Yang, 2016). Afterward, the obtained sensor (Apt/Cu_2O-CQDs/GCE) was immersed in the 3 ml PBS containing 1% BSA for 1 h to block some of the remaining active sites on the constructed sensor and also to reduce or eliminate undesired adsorption effects. Followed by each step, the prepared electrode washed with buffer solution to eliminate the excess of the physically and weakly adsorbed substances. To maintain the activity of the immobilized aptamers, the prepared aptasensor was kept into the buffer solution at 4 °C. By incubation of different concentrations of AFB1, the Apt/AFB1 complex was prepared on the modified electrode surface. The existence of AFB1 in solution prevented the electron transfer of the redox probe and so confirmed the formation of the Apt/AFB1 complex. The modification process and stability of the proposed nanoaptasensor was studied by EIS, CV, and DPV techniques. The schematic of the construction and performance stages of the proposed aptasensor is illustrated in Fig. 1.

2.6. The optimization of parameters by TM

The TM using the Minitab software is applied for design of experiments. In fact, it analyses the experimental data and optimizes different parameters of a system. Using this design, the smaller number of experiments is done rather than the traditional process. TM determines the finest amounts of the control parameters that affects the final signal. To get a complete understanding of factor effects, we assess the signal-to-noise ratios, because the aim of the experiments in this study is to maximize the AFB1 detection signal, so the TM uses the smaller signal-to-noise ratio (S/N). The S/N (smaller is the better), η can be expressed as (Phadke, 1995):

$$\eta = -10\log\left[\frac{1}{n}\sum y_i^2\right] \quad (1)$$

where η is S/N ratio 'y' is the observed data (potentiometric signal of aptasensor (I (μA)) and 'n' is the number of observations.

To decrease the experimental errors and enhance the reproducibility of experimental conditions, TM offers the Orthogonal Arrays (OA). Fractional designs decline the cost and time of the experiments. In this method, parameters are considered independently and the interactions between them are not considered. After completing the TM, analyzing the obtained data are employed to estimate the accuracy of selected parameters. Then, the optimal amounts of the control parameters selected and their performance was forecasted. The steps of this evaluation include the calculation of the S/N ratios from the empirical factors and difference in values for all parameters, identifying the best values, merge of all the optimum factors, forecasting of the S/N ratio obtained from signal of aptasensor by mathematical calculations and comparing it with the S/N ratio amount for experimental signal of aptasensor (the confidence level and maximum error are % 95 and ± 2σ, respectively). If the result is the same as the software forecasting, can be employed this collection of optimum amounts, and if there is too much difference, the chosen parameter must be modified.

2.7. Preparation of real samples

In this work, three wheat flour samples were randomly collected - from different bakeries (Kermanshah, Iran) and evaluated for the presence of AFB1 contamination. Firstly, 5 g of wheat flour samples was

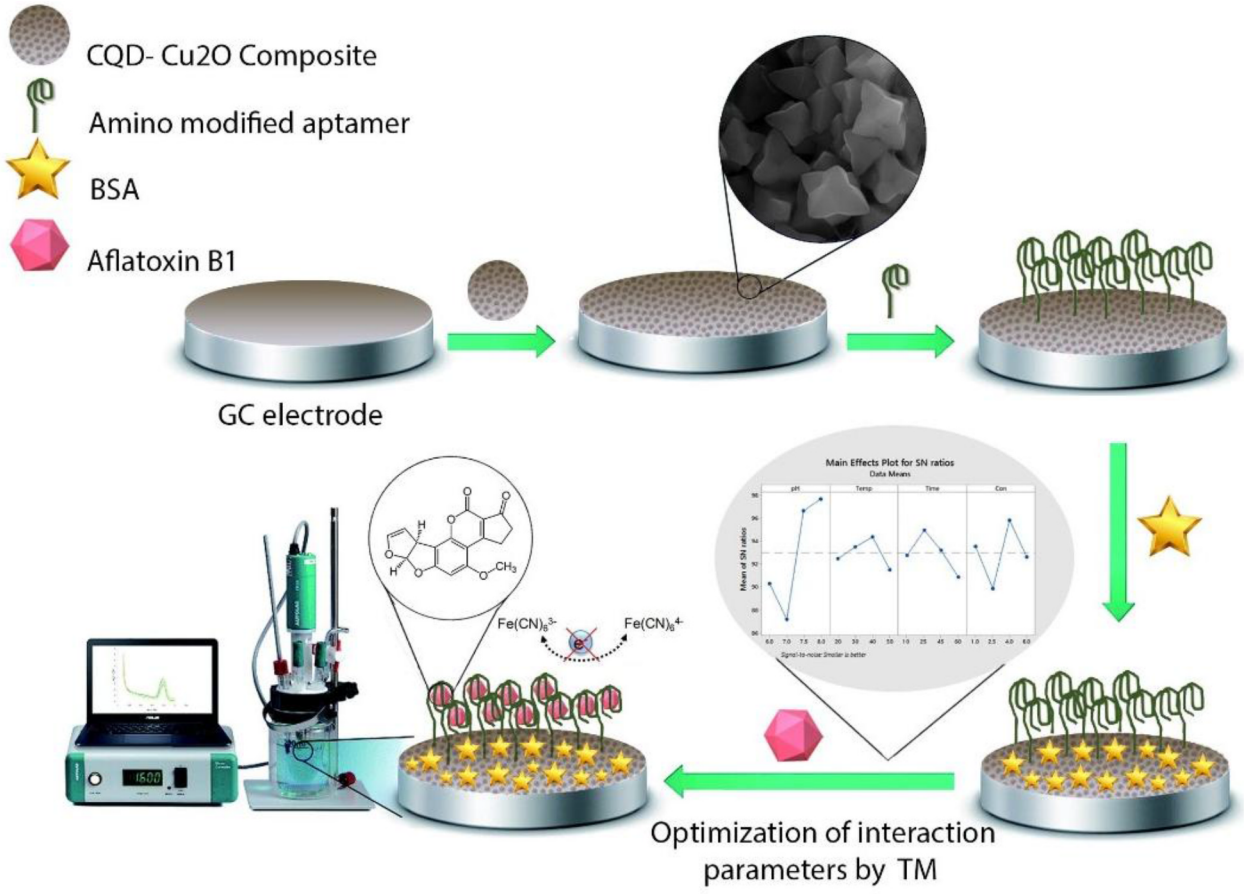

Fig. 1. Schematic of construction and performance stages of the proposed aptasensor.

taken and transferred individually into the three volumetric flasks. The wheat powders dissolved in 25 ml methanol and after vertexing for 15 min, separation and extraction of the sample's content were done. Then the acquired extract was then passed through a suitable filter. Finally, the supernatant was collected and then diluted to 250 ml with DDW. Afterward, 500 µl of this prepared sample was spiked for further electrochemical studies in the presence of the proposed sensor (Peng, Li, Cui, Qiu, Chen, & Huang, 2018).

3. Results and discussion

3.1. Nanostructure characterization

The synthesized octahedral Cu_2O and the Cu_2O-CQDs nanocomposite were characterized by EDS, XRD, FTIR and, SEM techniques. Fig. S1 corresponds to the data of EDS analysis related to the Cu_2O NPs and Cu_2O-CQDs nanocomposite surfaces (as shown in the supplementary materials). The EDS method is often applied to acquire a confined chemical analysis based on centralized emitted electrons from a solid sample bombarded as the X-ray spectrum. These spectra are not complicated and investigation of the lines is used for qualitative analysis. The obtained data from Fig. S1A and B illustrated the Cu_2O particles included mostly Cu as the main chemical element along with minor amounts of oxygen, demonstrating pure chemical composition of Cu_2O NPs structure. The Figs. S1C and D demonstrate the EDS analysis data of Cu_2O-CQDs nanocomposite. These results show Cu_2O particles are strongly attached to the surface of CQDs nanoparticles and also present the presence of the carbon in nanocomposite structures. As well as higher amounts of oxygen can be observed in the nanocomposite structure. The simultaneous use of both NPs is very important because of the great connection and also conduction of the network which can facilitate electron transfer.

Fig. 2A and B show the SEM images of octahedral Cu_2O and Cu_2O-CQDs composite. It is clear that the surface of Cu_2O-CQDs nanocomposites possess coarse surface unlike the octahedral Cu_2O NPs with smooth surface. These results illustrate the CQDs NPs in the first place coated the surface of Cu_2O NPs. Therefore, the Cu_2O particles and CQDs NPs would form good contact in the step.

Fig. 2**C** shows the XRD spectra of Cu_2O and Cu_2O-CQDs nanocomposite. This analysis is often used to determine the structure of the samples. There is a strong peak (1 1 1) of octahedral Cu_2O and CQDs/octahedral Cu_2O, which showed that the nanocrystals progressively formed with more surfaces and the surface of Cu_2O coating on CQDs do not change the octahedral configurations

Fig. S2 shows the FT-IR spectra of synthesized Cu_2O (curve a) and Cu_2O-CQDs composite (curve b). The IR absorption bands of free Cu_2O at 628 cm^{-1} and Cu_2O-CQDs nanocomposite at 629.49 cm^{-1} correspond to Cu–O vibrations. Nevertheless, it is more noteworthy that the characteristic hydroxyl groups (–OH) bonds at around 3434 and 3432.50 cm^{-1} in Cu_2O and nanocomposite structure, respectively (Ho, Tay, Qi, Huang, Li, & Chen, 2017). After the formation of Cu_2O-CQDs nanocomposite the intensity of the absorption band of hydroxyl groups increases, while the IR peaks of –OH groups at 3053 and 2960 cm^{-1} almost disappear. Also, the IR band of Cu_2O-CQDs composite at 1439 cm^{-1} corresponds to –C═O stretching vibrations that disappears completely in the spectrum of free Cu_2O. The other functional groups and chemical bonds of Cu_2O remain unchanged after the formation of the Cu_2O-CQDs nanocomposite (Alarfaj, El-Tohamy, & Oraby, 2018).

3.2. Electrochemical characterization

The Electrochemical Impedance Spectroscopy (EIS) procedure is mostly applied to evaluation for the changes that occurred on the interface of the electrode surface and solution. By exerting a sinusoidal potential in EIS examinations, and then quantification of the outcome current, the electrochemical impedance of an electrode is specified. The EIS spectrum consists of two configurations of layouts, Nyquist and Bode layouts. Bode layout is a graph amid the phase shift of the impedance and the absolute impedance, each of as a subordinate of frequency, which is a beneficial replacement to the Nyquist plot. In EIS measurements, $[Fe(CN)_6]^{3-/4-}$ has been often employed as a redox probe. In the EIS evaluations, the diameter of the semicircle at the high frequency part illustrates the value of electron transfer resistance (R_{et}). The R_{et} generally depicts the faradaic processes that occur at the electrode/electrolyte interface and shows the kinetic aspect of the electron transfer reaction of the redox species on the surface. Meanwhile, the straight line will appear in the low frequency region corresponds to the diffusion process of the redox species. Variation of the R_{et} value is dependent on nature of modifiers and the surface modification process (Liu, Lei, Huang, & Ju, 2014).

After modification of GCE at each step, important changes of the Nyquist plots for all electrodes (GCE (a), CQDs/GCE (b), Cu_2O/GCE (c), Cu_2O-CQDs/GCE (d), Apt/Cu_2O-CQDs/GCE (e) and BSA/Apt/Cu_2O-CQDs/GCE (f)) were obtained in the frequency range from 100 kHz to 0.1 Hz and at initial potential of 0.15 V in a KCl solution (0.1 M) containing $[Fe(CN)_6]^{3-/4-}$ (0.5 mM) (Fig. 3**)**. The inset of Fig. 3 shows an equipollent circuit used for modeling of impedance data in the attendance couple of redox. A semicircle domain with R_{et} is about 492 Ω was obtained for the Nyquist plot on the bare GCE (curve a), which the small amount for R_{et} depicted the redox probes provide the fast electron transfer rate on the surface of GCE. In the next step, on the surface of CQDs/GCE, the R_{et} value was significantly enhanced to 12400 Ω (curve b), which demonstrated the formation of the CQDs layer leads to the slow electron transfer between the surface and redox probe than the obtained result for bare GCE. Also, an enhancement in R_{et} value on the CQDs/GCE (curve b) may be was owing to the presence of negative charge of the modifier and so, the repulsive force between probe and CQDs with negative charge surface (Liu et al., 2014). Increasing the amounts of R_{et} up to 27,000 at the Cu_2O/GCE surface (curve c) indicates the less conductivity of Cu_2O (than CQD) can decrease the transfer rate of electron and so the redox species were diffused towards the surface with lower speed. After casting the nanocomposite of Cu_2O-CQDs on GCE surface, the R_{et} amount was reduced significantly up to 14000 Ω (curve d). This decline in the R_{et} amount was obviously illustrated the good attachment of nanocomposites on the GCE surface, which finally led to enhancement of the sensor surface conductivity (He et al., 2011). After immobilizing the aptamers at Cu_2O-CQDs/GCE surface, the R_{et} value of Apt/Cu_2O-CQDs/GCE largely increased (R_{et} = 35000 Ω, curve e), which depicted the immobilization of aptamers on the sensor surface and therefore, prevented the transfer of electrons in a redox reaction to the sensor surface. The coverage of the surface with the immobilized oligonucleotides as physical coverage led to the electrostatic interaction as repulsive effects between $[Fe(CN)_6]^{3-/4-}$ and negative charge localization on phosphate backbones in the DNA led to the decrease of electron transfer of redox species to the surface. Finally, by immersion of the prepared aptasensor of in a BSA solution the R_{et} value increased much more (R_{et} = 53000 Ω, curve f) due to successful immobilization of the BSA on the aptasensor surface such as immobilization of aptamers (Ghanbari, Roushani, & Azadbakht, 2017).

3.3. Optimization of analytical conditions by TM

The optimum conditions for measurement of the AFB1 were determined according to the Taguchi experimental design method using Minitab software. The 4-level designs based on the L16 orthogonal array (OA) in Minitab software, along with a selection of four factors of pH, temperature, time, and aptamer concentration have been accomplished (Table S1). The software calculates the values of the S/N ratio at the different conditions and obtains the optimum conditions based on smaller S/N ratios. The optimum conditions were obtained based on the results of the designed experiments in Table S2. The acquired optimum parameters in the theoretical results presented by TM have confirmed

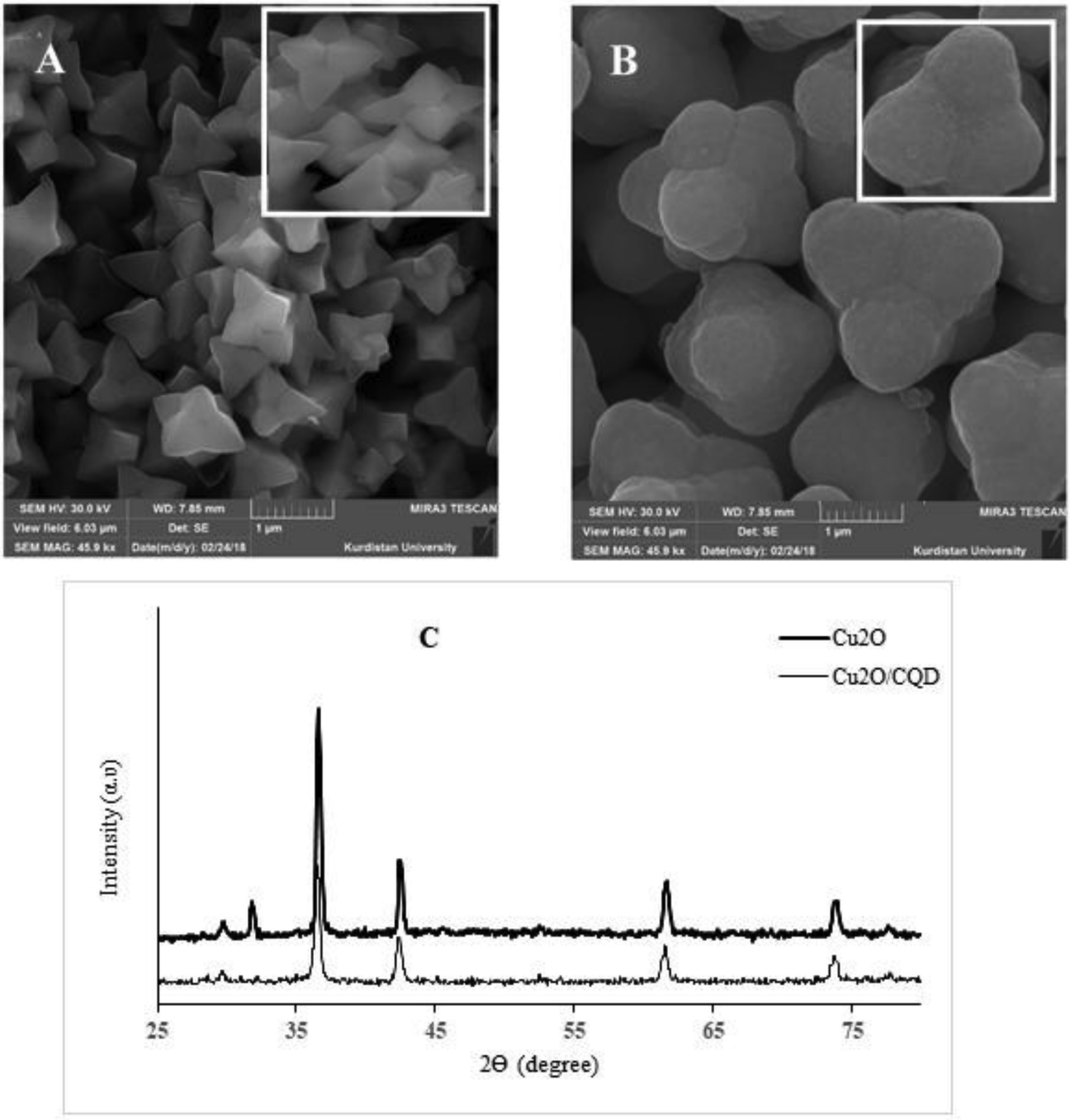

Fig. 2. The SEM images of synthesized Cu_2O (A) and Cu_2O-CQDs composite (B). XRD pattern of octahedral Cu_2O and CQDs/octahedral Cu_2O (C).

the optimum conditions in experimental results.

The effective factors usually have interactions with each other. Therefore, the effect of selected level factors on peak current was evaluated (Fig. 4). Better peak current was obtained with optimum factors as above mentioned and according to the results, the lines are not parallel to each other. Hence, by looking at the effects of each factor separately, the overall interactions between the factors and their influence on the signal of aptasensor can be distinguished. So, there is a specified relation among the effective factors. It can be expressed the all factors are affecting parameters in this analysis, and have the same and effective contribution on signal. Therefore, optimization based on the Taguchi experimental design provided a high model optimization that is closer to experimental signal values (Dar & Anuradha, 2018).

Also, responses were investigated by the 3D surface plots as shown in Figs. S3A and B. The response surface plots can be utilized to recognize the significant interactions between the experimental factors (Ashengroph, Nahvi, & Amini, 2013). The response of surface plots was drawn by the regression model to illustrate the composed influences of I_p versus the time and concentration (Fig. S3A), I_p versus the pH and temperature (Fig. S3B). The maximum I_p was obtained exactly based on the signals in the main effect plot (Fig. S4), which corroborated the interaction effects between the factors.

The contour plots also were analyzed to investigate the effect of the parameters on signals. By analyzing these plots, the impact of pH, temperature, time, and concentration as crucially, contribution factors described and depicted in **Figs. S3C and D**. From contour plots, a region of deep green color displays the highest response and in reverse, a region of light green color shows the lowest signal. An increase in I_p was

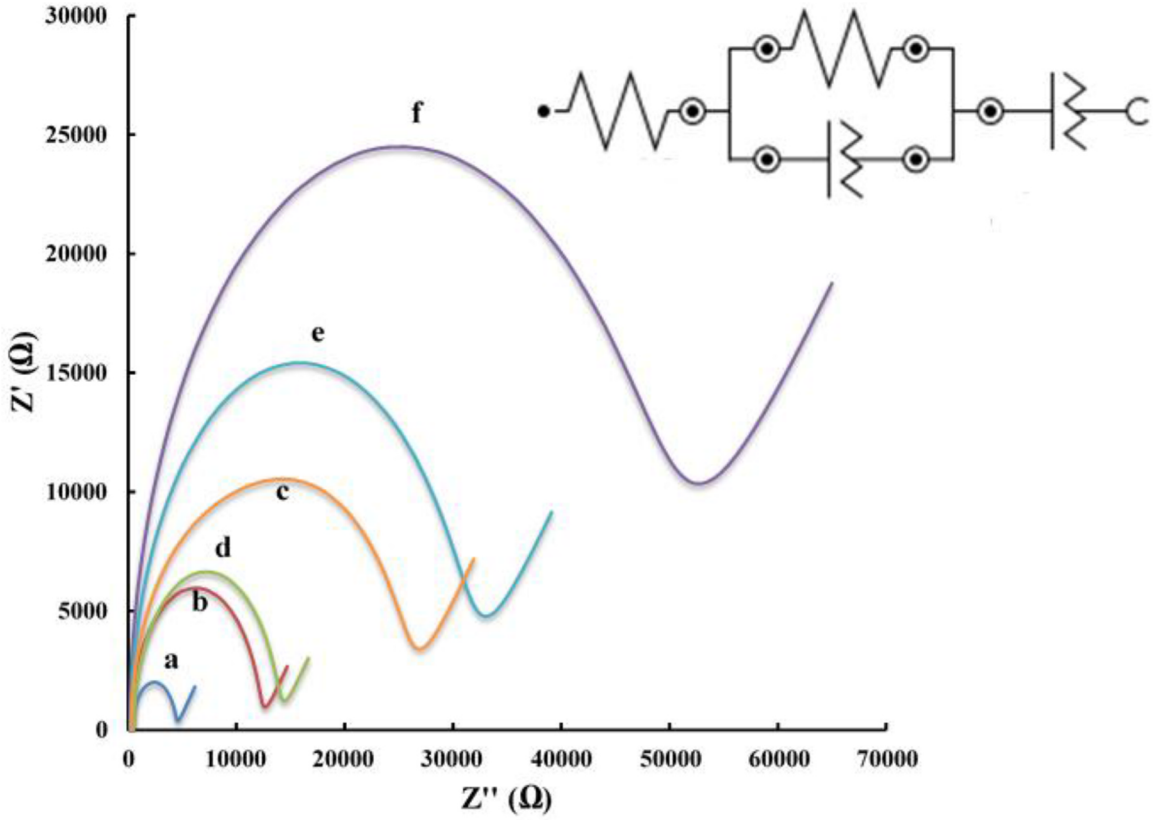

Fig. 3. The Nyquist plots of GCE (curve a), CQDs/GCE (curve b), Cu_2O/GCE (curve c), Cu_2O-CQDs/GCE (curve d), Apt/Cu_2O-CQDs/GCE (curve e) and BSA/Apt/Cu_2O-CQDs/GCE (curve f). Conditions: frequency range of 100 kHz to 0.1 Hz at potential, 0.15 V. Inset: An equipollent circuit utilized for modeling of impedance data in the attendance couples of redox.

associated with an enhancement in time between 40 and 50 min and an increase of concentration between 2 and 3 μM (**Fig. S3C**), that illustrated with a white arrow. Then out of this range, the decline was observed for I_p with a further enhancement of. Temperature and concentration. As well as, for factors of pH and temperature, the observed behaviors of these parameters were identically according to the results in the main effect plot (**Fig. S4**). Furthermore, the interaction effects between factors in addition to the linear effects of them lead to curvature form (circular and elliptical plot) in contour plots (Dash, Mohammed, & Humaira, 2016). These results confirmed exactly optimal levels for the main effect plot (**Fig. S4**) as explained above. According to this data, the pH = 7.0, temperature = 50 °C, time = 45 min and aptamer concentration = 2.5 μM have been chosen as the optimum analysis conditions.

Since the aptamer is a biological substance, therefore investigations should be the way that the aptamer will not be damaged. Therefore, all of the tests were accomplished in a PBS with a pH of 7.0 which is a neutral medium. This quantity corresponds with previous research (Abnous et al., 2017; Castillo, Spinella, Poturnayová, Šnejdárková, Mosiello, & Hianik, 2015; Geleta et al., 2018; Goud, Catanante, Hayat, Satyanarayana, Gobi, & Marty, 2016; Wu et al., 2019; Zheng et al., 2016). The effect of the interaction temperature between AFB1 and the aptamers was studied. The experimental results illustrated the signal was enhanced with the increase of incubation temperature up to 50 °C and higher temperatures did not increase the signal with clarity. So, 50 °C was selected as the optimum temperature in the subsequent evaluations. The incubation during the time of AFB1 with the aptamer was also optimized. These parameters are significant parameters for the binding of AFB1 with the aptamers on the surface. The experimental results depicted the signal was enhanced with the increasing of time up to 45 min and a great amount of incubation time did not lead to enhancement of the signal at the aptasensor. So, 45 min was chosen as the most favorable amount for incubation time to the interaction between AFB1 and aptamer on the surface. To optimize the immobilized dosage of aptamer, different concentrations of aptamer immobilized on the electrode surface. There is an increasing trend up to higher concentrations than 2.5 μM due to surface saturation and so, the optimum concentration was chosen to be 2.5 μM for the next experiments.

3.4. Analytical parameters of Apt/Cu_2O-CQDs/GCE biosensor

3.4.1. Evaluation of the linear Range, limit of detection (LOD) and limit of quantification (LOQ)

The analytical performance of offered aptasensor has been measured by probing the DPV signals of $[Fe(CN)_6]^{3-/4}$ after incubation with the different concentrations of AFB1 for 45 min in PBS (pH = 7.0) (Fig. 5**A**). The results illustrate the AFB1 has a great attachment to aptamers at the surface of the sensor. Therefore, as expected the anodic peak current decreases with enhancement of concentrations of the AFB1, indicating the formation adduct of Apt-AFB1 (between aptamers and AFB1) and preventing the electron transfer of $[Fe(CN)_6]^{3-/4}$ to the electrode surface. A linear calibration curve between 3 ag ml^{-1} and 1.9 μg ml^{-1} with a regression equation of ΔI (μM) = 7.5761 log C_{AFB1} + 42.442 (R^2 = 0.9921) was obtained. The LOD (0.9 ag ml^{-1}) was calculated via $3S_b$ /m, which S_b and m are the standard deviation of the blank signal and the slope of the calibration diagram, respectively (Fig. 5**B**). In addition, the limit of quantification (LOQ) was also calculated via 10 S_b/m, it was equal to 3.0 ag ml^{-1}.

The proposed electrochemical aptasensor shows a higher sensitivity compared with the other offered aptasensors for AFB1 detection (Table 1) (Abnous et al., 2017; Castillo et al., 2015; Geleta et al., 2018; Goud et al., 2016; Wu et al., 2019; Zheng et al., 2016). This result

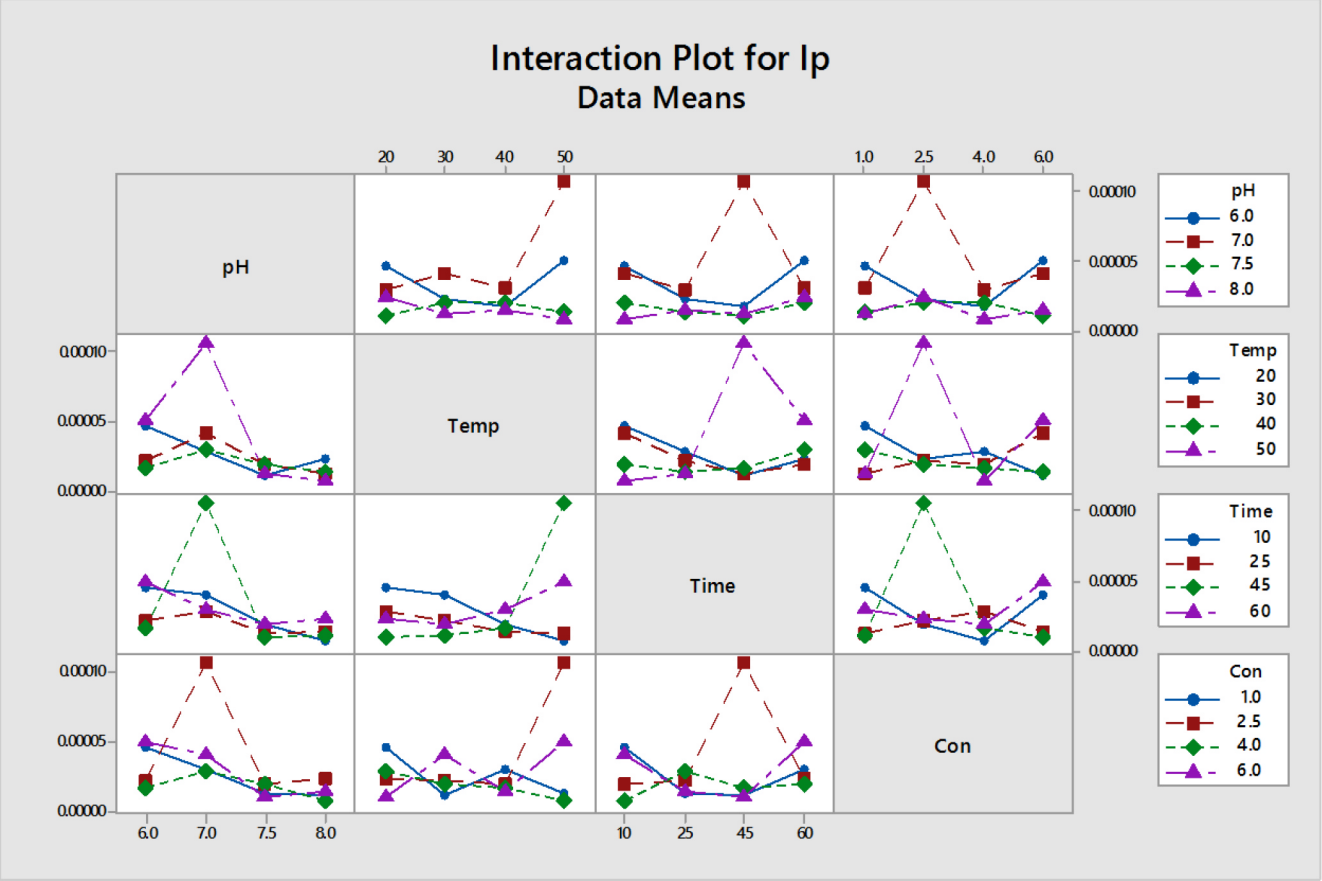

Fig. 4. Interaction plot for I_p by data means of pH, aptamer concentration, temperature and incubation time.

(LOD = 0.9 ± 0.04) is achieved by performing 10 replicate measurements. This finding can be due to the more performed active sites and the large surface area of the applied nanocomposite. Indeed, exerting the offered nanocomposite combined the independent properties of CQDs and Cu_2O nanomaterials, which led to the eminence of designed aptasensor for AFB1 detection.

3.4.2. Evaluation of aptasensor specificity

The specificity of the designed aptasensor is one of its most important features, which indicates that what extent of the response of the

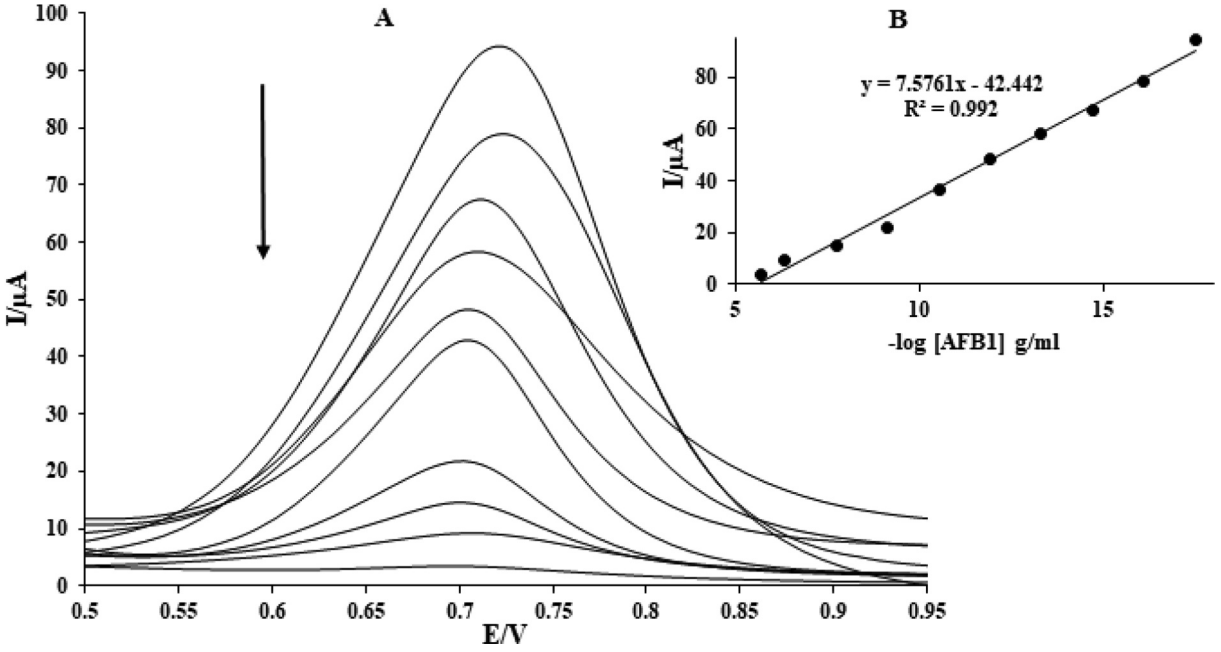

Fig. 5. (A) The DPVs of $[Fe(CN)_6]^{3-/4}$ after aptasensor incubation with different concentrations of AFB1 (3 ag ml^{-1} – 1.9 µg ml^{-1}), (B) The linear relationship between current vs. logarithmic concentration of AFB1 in a solution PBS (pH = 7.0).

Table 1
Comparison of the performances of various AFB1 aptasensors.

Electrode	Linear range	LOD	Conditions	Real sample	References
GCE/RGO/MoS_2/PANI@AuNPs/Apt [a]	0.01–1.0 fg/ml	0.002 fg/ml	PBS (pH = 7.5)	Wine	(Abmous et al., 2017)
Fc-cDNA/pβ-CD/AuNPs/GCE [b]	0.1 pg/ml- 10 ng/ml	0.049 pg/ml	PBS (pH = 7.4)	peanut oil	(Castillo et al., 2015)
Apt/PAMAM G4/GA/Cys/AuE [c]	0.03–3 ng/ml	124 ng/ml	PBS (pH = 7.4)	peanuts	(Evtugyn et al., 2014)
SPCE/4-CP/Apt [d]	0.125 ng/ml-16 ng/ml	0.12 ng/ml	PBS (pH = 7.4)	Beer, Wine	(Geleta et al., 2018)
Apt/NR-TCA/GCE [e]	0.03–30 ng/ml	0.015 ng/ml	HEPES (pH = 7.0)	Foodstuffs	(Goud et al., 2016)
Apt1/S-primer-AuNP-cDNA/dNTP/MB/EXOIII/AuE [f]	0.09–940 ng/ml	0.05 ng/ml0.05 ng/ml	PBS (pH = 7.4)	–	(Wu et al., 2019)
Apt-CSs-modified electrod/Exo I /GCE [g]	7–500 pg/ml	2 pg/ml	$[Fe(CN)_6]^{3-/4-}$ (3 mM)	Serum, Grape juice	(Zheng et al., 2016)
Apt/Cu_2O-CQDs/GCE	3 Ag/ml-1.9 μg/ml	0.9 Ag/ml	PBS (pH = 7.5)	Wheat flour	This work

[a] Glassy carbon electrode/reduced graphene oxide/molybdenum disulfide/polyaniline@gold nanoparticles; [b] Fc-labeled aptamer/β-cyclodextrin/gold nanoparticles/glassy carbon electrode; [c] Aptamer/poly (amidoamine) dendrimers of fourth generation/glutaraldehyde/cystamine/gold electrode; [d] screen printed carbon electrodes/4-carboxyphenyl/aptamer; [e] Aptasensor based on polycarboxylic macrocycle (thiacalix[4]arene) modified with neutral red/GCE; [f] Aptamer 1/thiol-modified telomerase primer-goldnanoparticles-single stranded capture DNA/telomerase extracts/methylene blue/exonuclease III/gold electrode; [g] Aaptamer-complementary strands of aptamer complexes/exonuclease I/gold electrode.

sensor is to an intended analyte than the other compounds or interferences. To investigate the analytical applicability of the proposed way for AFB1 detection, the results of several possible interfering compounds have been studied under optimum conditions. The effects of some interfering common toxins including zearalenone (ZEN), ochratoxin A (OTA), AFB2, and AFM1 were studied using the DPV method in the presence of AFB1 (3 ng ml^{-1}) at 10-fold higher concentrations of interferences than AFB1. Based on these data, not observed any changes to the aptasensor response. The RSD measured less than 5% for the above interferences. These data show the acceptable selectivity of the procedure and so it is appropriate for AFB1 detection in food samples with different matrices (Table S3).

3.4.3. Evaluation of Precision: Repeatability and reproducibility

The repeatability was investigated by consecutive measurements of 0.800 μg ml^{-1} of AFB1 for six times using the Apt/Cu_2O-CQDs/GCE independently. The relative standard deviation (RSD) was measured as 2.4%, which illustrates a high repeatability and admissible precision (**Fig.S5A).**

Furthermore, aptasensor reproducibility was evaluated by measuring the AFB1 content on six different days (Table S4). The average AFB1 content was 0.804 M with a 2.56% RSD.

3.4.4. Evaluation of robustness

Robustness is defined as the ability to reproduce the analytical method under different situations without the occurrence of meaningful differences in the results.

In this specific case, robustness refers to the entire process from the fabrication of the aptasensor to the final AFB1 measurement. In order to test the method robustness, four new aptasensors were built; for each aptasensor Cu_2O nanoparticles, CQDs and their nanocomposites were synthesized again to obtain new electrodes, aptamer solution was freshly prepared for each individual biosensor and the AFB1 concentration in the sample was measured using each one of the four biosensors. Therefore, all the factors that could affect the fabrication of the biosensor were considered in the robustness test. These four new aptasensors were used to quantify the AFB1 present in the sample over four different days. The RSD of the robustness test was measured 3.25% **(Fig, S5B)**. This value indicates that the whole method, including the sensor construction and the measurement process is repeatable, reproducible, and robust.

3.4.5. Evaluation of stability

One of the most important and critical parameters in evaluating the performance of the aptasensors is their long-term stability. After preparing of aptasensor and storing at 4 °C, the clear changes of the signal were not observed to detect the same AFB1 concentration after storing for 19 days, which shows the stability of this proposed sensor. Also, after recording the 13 successive scans, only 96% decrement of the primary signal was detected (**Fig. S5C**). These findings show the good long-term stability and sensitivity of the aptasensor.

3.4.6. Evaluation of accuracy and reliability

To evaluate the reliability and accuracy of the proposed aptasensor, it was used to detect AFB1 in wheat flour samples. The spiked solution with different concentrations of AFB1 were examined using standard addition method. The recoveries were calculated using added and found values (Table S5**).** The recovery values for the detection of AFB1 were obtained in the range of 97.2–104.4% indicating the potential of the offered aptasensor to detect the AFB1 in real samples.

3.4.7. Trueness

Trueness is the closeness of agreement between the average value obtained from a large set of test results and an accepted reference value (Magnusson, 2014).

In the simplest way, it can be estimated by analyzing suitable Certified Reference Materials (CRMs). In such a case, one can carry out an adequate series of measurements of the CRM and then perform a simple *t*-test for the comparison of the experimental mean with the certified value (Eq. (2)):

$$t_{exp} = \frac{|x_{mean} - C_{CRM}|.\sqrt{N}}{s} \quad (2)$$

Where x_{mean} and C_{CRM} are the experimental mean relevant to the analysis of the CRM and the certified value, respectively, N is the number of samples, and s is the standard deviation. If t_{exp} exceeds the critical two-tail *t*-value for N-1 degrees of freedom and the selected confidence level, P, then one can reject the hypothesis of the absence of a difference between x_{mean} and C_{CRM}.

The value of t_{exp} was obtained based on the data in Table S6, which is equal to 0.062164. Since this value is smaller than the value of t_{table} in the confidence level of 0.95 and in the degree of freedom 9 (0.064477), the null hypothesis is proved and there is no significant error in the obtained data. Furthermore, using the data in Table S6, the confidence interval was obtained at the confidence level of 0.95 and the degree of freedom 9, which due to the fact that the average value is in the confidence interval calculated using the following equation, no significant error approved.

$$Confidence\ \ interval = \mu \mp \frac{ts}{\sqrt{N}} \quad (3)$$

where μ is the certified value (C_{CRM} in Eq. (2)), t is the maximum permissible error in a data set at the specified confidence level, s is the standard deviation and N is the number of samples.

Other statistical parameters such as RSD, Mean Absolute Error (MAE) and variance of these results were also calculated Table S6, which indicates the absence of random and significant error in the results.

4. Conclusion

In summary, we have constructed an electrochemical aptasensor based on Cu_2O-CQDs nanocomposite for the detection of AFB1. In this work, we used taguchi method as an advantageous tool to find the optimum parameters to reduce the number of experiments and saving time and reagents.

To take the benefits of nanocomposite including large surface area, increase the immobilization efficiency of aptamer and also finding the best condition for experiments by taguchi method, the offered aptasensor displays acceptable reproducibility, good stability, excellent sensitivity (low detection limits with a wide linear range from 3 $ag.ml^{-1}$ to 1.9 $\mu g.ml^{-1}$ in PBS buffer solution) and high selectivity for detection of low amounts of the AFB1. Furthermore, the results of statistical parameters confirmed the acceptable accuracy and precision of the aptasensor.

Declaration of Competing Interest

The authors declare that they have no known competing financial interests or personal relationships that could have appeared to influence the work reported in this paper.

Appendix A. Supplementary data

Supplementary data to this article can be found online at https://doi.org/10.1016/j.foodchem.2020.128436.

References

Abnous, K., Danesh, N. M., Alibolandi, M., Ramezani, M., Emrani, A. S., Zolfaghari, R., & Taghdisi, S. M. (2017). A new amplified π-shape electrochemical aptasensor for ultrasensitive detection of aflatoxin B1. *Biosensors and Bioelectronics, 94*, 374–379.

Alarfaj, N. A., El-Tohamy, M. F., & Oraby, H. F. (2018). CA 19–9 pancreatic tumor marker fluorescence immunosensing detection via immobilized carbon quantum dots conjugated gold nanocomposite. *International Journal of Molecular Sciences, 19*(4), 1162.

Ashengroph, M., Nahvi, I., & Amini, J. (2013). Application of Taguchi design and Response surface methodology for improving conversion of isoeugenol into vanillin by resting cells of Psychrobacter sp. *CSW4. Iranian Journal of Pharmaceutical Research: IJPR, 12*(3), 411.

Athreya, S., & Venkatesh, Y. (2012). Application of Taguchi method for optimization of process parameters in improving the surface roughness of lathe facing operation. *International Refereed Journal of Engineering and Science, 1*(3), 13–19.

Azri, F. A., Selamat, J., & Sukor, R. (2017). Electrochemical immunosensor for the detection of aflatoxin B1 in palm kernel cake and feed samples. *Sensors, 17*(12), 2776.

Castillo, G., Spinella, K., Poturnayová, A., Šnejdárková, M., Mosiello, L., & Hianik, T. (2015). Detection of aflatoxin B1 by aptamer-based biosensor using PAMAM dendrimers as immobilization platform. *Food Control, 52*, 9–18.

Dar, A., & Anuradha, N. (2018). Use of orthogonal arrays and design of experiment via Taguchi L9 method in probability of default. *Accounting, 4*(3), 113–122.

Dash, R. N., Mohammed, H., & Humaira, T. (2016). An integrated Taguchi and response surface methodological approach for the optimization of an HPLC method to determine glimepiride in a supersaturatable self-nanoemulsifying formulation. *Saudi pharmaceutical journal, 24*(1), 92–103.

Farmani, M. R., Peyman, H., & Roshanfekr, H. (2020). Blue luminescent graphene quantum dot conjugated cysteamine functionalized-gold nanoparticles (GQD-AuNPs) for sensing hazardous dye Erythrosine B. *Spectrochimica Acta Part A: Molecular and Biomolecular Spectroscopy, 229*, Article 117960.

Geleta, G. S., Zhao, Z., & Wang, Z. (2018). A novel reduced graphene oxide/molybdenum disulfide/polyaniline nanocomposite-based electrochemical aptasensor for detection of aflatoxin B 1. *Analyst, 143*(7), 1644–1649.

Ghanbari, K., Roushani, M., & Azadbakht, A. (2017). Ultra-sensitive aptasensor based on a GQD nanocomposite for detection of hepatitis C virus core antigen. *Analytical biochemistry, 534*, 64–69.

Goud, K. Y., Catanante, G., Hayat, A., Satyanarayana, M., Gobi, K. V., & Marty, J. L. (2016). Disposable and portable electrochemical aptasensor for label free detection of aflatoxin B1 in alcoholic beverages. *Sensors and Actuators B: Chemical, 235*, 466–473.

Hashemi, M., & Taherimaslak, Z. (2014). Separation and determination of aflatoxins B 1, B 2, G 1 and G 2 in pistachio samples based on magnetic solid phase extraction followed by high performance liquid chromatography with fluorescence detection. *Analytical Methods, 6*(19), 7663–7673.

Hashemi, M., Taherimaslak, Z., & Rashidi, S. (2014). Application of magnetic solid phase extraction for separation and determination of aflatoxins B1 and B2 in cereal products by high performance liquid chromatography-fluorescence detection. *Journal of Chromatography B, 960*, 200–208.

He, X., Li, H., Liu, Y., Huang, H., Kang, Z., & Lee, S.-T. (2011). Water soluble carbon nanoparticles: Hydrothermal synthesis and excellent photoluminescence properties. *Colloids and Surfaces B: Biointerfaces, 87*(2), 326–332.

Hernandez-Vargas, H., Castelino, J., Silver, M. J., Dominguez-Salas, P., Cros, M.-P., Durand, G., ... Moore, S. E. (2015). Exposure to aflatoxin B1 in utero is associated with DNA methylation in white blood cells of infants in The Gambia. *International Journal of Epidemiology, 44*(4), 1238–1248.

Heydarzadeh, S., Roshanfekr, H., Peyman, H., & Kashanian, S. (2020). Modeling of ultrasensitive DNA hybridization detection based on gold nanoparticles/carbon-nanotubes/chitosan-modified electrodes. *Colloids and Surfaces A: Physicochemical and Engineering Aspects, 587*, Article 124219.

Ho, W. C. J., Tay, Q., Qi, H., Huang, Z., Li, J., & Chen, Z. (2017). Photocatalytic and adsorption performances of faceted cuprous oxide (Cu2O) particles for the removal of methyl orange (MO) from aqueous media. *Molecules, 22*(4), 677.

Ilgu, M., & Nilsen-Hamilton, M. (2016). Aptamers in analytics. *Analyst, 141*(5), 1551–1568.

Li, Y., Zhong, Y., Zhang, Y., Weng, W., & Li, S. (2015). Carbon quantum dots/octahedral Cu2O nanocomposites for non-enzymatic glucose and hydrogen peroxide amperometric sensor. *Sensors and Actuators B: Chemical, 206*, 735–743.

Liu, L., Jin, H., Sun, L., Ma, S., & Lin, R. (2012). Determination of Aflatoxins in Medicinal Herbs by High-performance Liquid Chromatography-Tandem Mass Spectrometry. *Phytochemical Analysis, 23*(5), 469–476.

Liu, Y., Lei, J., Huang, Y., & Ju, H. (2014). "Off-on" electrochemiluminescence system for sensitive detection of ATP via target-induced structure switching. *Analytical Chemistry, 86*(17), 8735–8741.

Magnusson, B. (2014). The fitness for purpose of analytical methods: a laboratory guide to method validation and related topics (2014). Eurachem.

Miao, H., Wang, L., Zhuo, Y., Zhou, Z., & Yang, X. (2016). Label-free fluorimetric detection of CEA using carbon dots derived from tomato juice. *Biosensors and Bioelectronics, 86*, 83–89.

Mirian, M., Khanahmad, H., Darzi, L., Salehi, M., & Sadeghi-Aliabadi, H. (2017). Oligonucleotide aptamers: Potential novel molecules against viral hepatitis. *Research in Pharmaceutical Sciences, 12*(2), 88.

Mishra, G. K., Sharma, V., & Mishra, R. K. (2018). Electrochemical aptasensors for food and environmental safeguarding: A review. *Biosensors, 8*(2), 28.

Peng, G., Li, X., Cui, F., Qiu, Q., Chen, X., & Huang, H. (2018). Aflatoxin B1 electrochemical aptasensor based on tetrahedral DNA nanostructures functionalized three dimensionally ordered macroporous MoS2–AuNPs film. *ACS Applied Materials & Interfaces, 10*(21), 17551–17559.

Phadke, M. S. (1995). *Quality Engineering Using Robust Design.* Prentice Hall PTR.

Pyman, H., Roshanfekr, H., & Ansari, S. (2020). DNA-based electrochemical biosensor using chitosan–carbon nanotubes composite film for biodetection of Pirazon. *Iranian Chemical Communication, 8*(1), 52–64.

Sharma, V., Hynek, D., Trnkova, L., Hemzal, D., Marik, M., Kizek, R., & Hubalek, J. (2016). Electrochemical determination of adenine using a glassy carbon electrode modified with graphene oxide and polyaniline. *Microchimica Acta, 183*(4), 1299–1306.

Wang, L., Zhao, J., He, X., Gao, J., Li, J., Wan, C., & Jiang, C. (2012). Electrochemical impedance spectroscopy (EIS) study of LiNi1/3Co1/3Mn1/3O2 for Li-ion batteries. *Int. J. Electrochem. Sci, 7*(1), 345–353.

Wu, S. S., Wei, M., Wei, W., Liu, Y., & Liu, S. (2019). Electrochemical aptasensor for aflatoxin B1 based on smart host-guest recognition of β-cyclodextrin polymer. *Biosensors and Bioelectronics, 129*, 58–63.

Yagati, A. K., Chavan, S. G., Baek, C., Lee, M.-H., & Min, J. (2018). Label-free impedance sensing of aflatoxin B1 with polyaniline nanofibers/Au nanoparticle electrode array. *Sensors, 18*(5), 1320.

Zhang, X., Li, C.-R., Wang, W.-C., Xue, J., Huang, Y.-L., Yang, X.-X., ... Ding, S.-J. (2016). A novel electrochemical immunosensor for highly sensitive detection of aflatoxin B1 in corn using single-walled carbon nanotubes/chitosan. *Food chemistry, 192*, 197–202.

Zheng, W., Teng, J., Cheng, L., Ye, Y., Pan, D., Wu, J., ... Chen, W. (2016). Hetero-enzyme-based two-round signal amplification strategy for trace detection of aflatoxin B1 using an electrochemical aptasensor. *Biosensors and Bioelectronics, 80*, 574–581.